Melt Spinning of β-Phase Poly(vinylidene fluoride) Yarns With and Without a Conductive Core

Anja Lund,[1,2] Bengt Hagström[3]

[1]*The Swedish School of Textiles, University of Borås, SE-501 90 Borås, Sweden*
[2]*Department of Materials and Manufacturing Technology, Chalmers University of Technology, SE-412 96 Göteborg, Sweden*
[3]*Swerea IVF, Textiles and Plastics Department, SE-431 22 Mölndal, Sweden*

Received 14 April 2010; accepted 21 August 2010
DOI 10.1002/app.33239
Published online 8 November 2010 in Wiley Online Library (wileyonlinelibrary.com).

ABSTRACT: When poly(vinylidene fluoride) (PVDF) is to be used as a piezoelectric material, the processing must include the formation of polar β-phase crystallites, as well as the application of electrically conducting charge collectors, that is, electrodes. In this article, results from the melt spinning of PVDF yarns and a novel bicomponent PVDF-yarn with a conductive carbon black/polypropylene (CB/PP) core are presented. Melt spinning has been done under conditions typical for industrial large-scale fiber production. The effects on the resulting crystalline structure of varying the spinning velocity, draw rate, and draw temperature are discussed. The results show that, for maximum α-to-β phase transformation, cold drawing should take place at a temperature between 70 and 90°C, and both the draw ratio and the draw rate should be as high as possible. It was observed that the cold drawing necessary to form β-phase crystallinity simultaneously leads to a decrease in the core conductivity of the bicomponent yarns. In this work, the melt spinning of bicomponent fibers with high-β-phase PVDF in the sheath and a CB/PP core was successfully accomplished. The core material remained electrically conductive, paving the way for the use of a CB-polymer compound as inner electrode in the melt spinning of piezoelectric bicomponent fibers. © 2010 Wiley Periodicals, Inc. J Appl Polym Sci 120: 1080–1089, 2011

Key words: fibers; WAXS; morphology

INTRODUCTION

In this article, we present results from the melt spinning of poly(vinylidene fluoride) (PVDF) yarns using an industrial scale spinning machine. PVDF is polymorphic and exists in at least four different crystal forms or phases designated α, β, γ, and δ.[1–10] When PVDF is processed to form films or fibers from the melt, the formation of the α-phase predominates. The α-phase is nonpolar and is undesirable for piezoelectric effects. The β-phase on the other hand is highly polar and is the most desirable crystalline form of PVDF for piezoelectric applications. The piezoelectric constant d_{33} of PVDF increases with the increasing fraction of β-phase crystallites.[11] In this work, yarns with an electrically conductive core serving as an inner electrode are spun toward a high content of the piezoelectric β-phase. The experimental work is largely based on results reported in our previous work,[12] where a more extensive overview of the molecular structure development during the film- and fiber-processing of PVDF is presented.

Correspondence to: A. Lund (anja.lund@hb.se).

Journal of Applied Polymer Science, Vol. 120, 1080–1089 (2011)

To date, the research reported on piezoelectric fibers is mostly related to ceramic fibers for use in composite materials. A few examples will be reviewed here. In one study,[13] continuous fibers of lead–zirconate–titanate (PZT) were produced by a suspension spinning process, woven into a large area planar fabric, and embedded in a polymer matrix. Silver paint was applied on both surfaces of the composite to form electrodes, and the piezoelectric properties were measured. It was seen that a soft matrix resulted in a higher piezoelectric strain constant (d_{33}) than a hard matrix, due to the greater mechanical compliance and better stress transfer to the ceramic phase. Furthermore, for efficient poling, it was important to have a good contact between fibers in the composite. Possible suggested applications include hydrophones, transducers, sensors, actuators, and vibration/noise cancellation. Other researchers[14] have produced PZT-fibers with a metal core to serve as inner electrode, both by extrusion, and hydrothermal (PZT nucleated and grown on a titanium substrate) methods. The fibers were embedded in a polymer matrix, which also contained carbon fibers (CFs). The CF/polymer composite constituted the outer electrode. The composites were tested for use as both sensors and actuators and found to be useful for the suppression of resonance vibration. The authors pointed out the importance of

manufacturing fibers with a small diameter for minimal inclusion effects in the composite. PZT-fibers have also been studied in applications for power generation.[15] Plates of PZT fibers embedded in an epoxy resin were manufactured, where the plate thickness direction coincided with the fiber axis direction. A number of different plates with different thicknesses, and containing fibers of different diameters, were electroded and poled. Power generation experiments showed that a maximum peak voltage of 350 V, corresponding to a peak power of 120 mW, could be obtained. The output voltage and power increased with increasing plate thickness and decreasing fiber diameter, and d_{33} increased with increasing plate thickness but was not affected by the fiber diameter. A sophisticated way to add electrodes to PZT fibers in active fiber composites is to use interdigitated electrodes (IDEs); arrays of conductors applied perpendicular to the fiber direction on both sides or along the circumference of the fiber. The IDEs are then embedded in a polymer matrix together with the fibers. IDEs may be metallic or made from conducting polymer.[16]

Using PVDF instead of PZT as the base for a piezoelectric material will introduce some important differences. As mentioned, polar β-phase crystallites must be formed. Also, poling in a very high-electric field (30–120 MV/m[17]) is required to align the crystallites. The design of the electrodes will be an important issue; as the expected output voltage from a PVDF sensor will be relatively low, it should be advantageous to use electrodes, which cover the whole surface of the PVDF and have a maximum overlap area for maximum charge collection. In commercially available PVDF-based piezoelectric coaxial cables,[18] a copper wire (the inner electrode) is surrounded by either an extruded poly(vinylidene fluoride-trifluoroethylene) [P(VDF-TrFE)] layer or a wound-up film of PVDF. A copper braid constitutes the outer electrode. The copolymer P(VDF-TrFE) crystallizes into the β-phase polymorph directly from the melt. In a study of the manufacture of piezoelectric PVDF coaxial cables,[19,20] it was shown to be possible to extrude a cable, which could then be drawn to induce the necessary β-phase, provided a suitable material was chosen for the cable's inner electrode. Suggested materials included highly plastic semiconducting polymers and fusible metals with a low-melting point. Applying the outer electrode also presented a difficulty, as applying a semiconducting thermoplastic polymer onto a conventional extrusion line normally requires a high temperature, which may in part destroy the β-phase crystallites. It was shown to be possible to modify the process line to decrease the effect of high temperature on the cable and eventually apply an outer electrode with a negligible change in β-phase content. Four methods (thermoelectret, breakdown, plasma, and corona) for poling the cable were then evaluated, and it was found that cables poled using the plasma method showed the highest value of piezoelectric constant (d_{3h}), whereas corona treatment was the second best method. Suggested applications include street traffic monitoring and alarm systems.

We believe that PVDF-based piezoelectric fibers or yarns would have advantages such as small diameter, low weight, high flexibility, and being virtually endless as well as easy to produce. Such fibers could be used both as single fiber miniature devices and in large area sensors or actuators, manufactured by common textile production methods such as weaving or knitting.

Results from our previous study[12] showed that PVDF fibers with a high degree of β-phase crystallinity could be produced by melt spinning. It was found that, using a high-melt draw ratio (MDR), fibers were produced with a high degree of crystallinity and that a high-draw ratio in cold drawing (λ) gave a high degree of β-phase crystallites. However, the higher the MDR, the lower is the maximum available λ. The experiments in our previous study were performed on small-scale laboratory equipment at spinning velocities far lower than that used in industrial spinning. Because the results showed that the velocities used in spinning and drawing were important factors for β-phase formation, it is relevant to extend the study to melt spinning using a larger scale spinning machine with higher extrusion and drawing velocities.

The aim of the work described in this article is to study the melt spinning of PVDF under conditions typical for industrial-scale fiber production. In particular, the effects on the resulting crystalline structure of varying the spinning velocity, draw rate, and draw temperature have been investigated. Early results from the melt spinning of a novel bicomponent yarn with an outer layer of β-phase PVDF and a conductive core, which can be used as inner electrode, are also presented.

MATERIALS AND METHODS

Materials

The polymers used were commercially available homopolymer grades of PVDF and polypropylene (PP). The PVDF was Solef 1008/0001 (Solvay Solexis, Milan, Italy). The molecular weights as given by the supplier were $M_n = 114 \times 10^3$ Da or $M_w = 244 \times 10^3$ Da, and the average melt flow index (MFI) was 8 g/10 min under a load of 2.16 kg at 230°C. The density was 1.78 g/cm^3 in the solid state and 1.416 g/cm^3 in the molten state (at 250°). The PP was HG245FB (Borealis, Stenungsund, Sweden), with

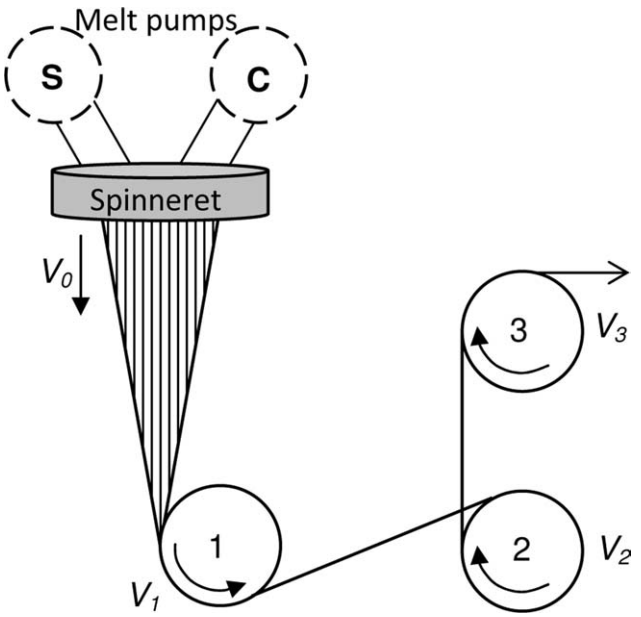

Figure 1 Schematic description of the ESL fiber spinning machine.

MFI = 26 g/10 min under a load of 2.16 kg at 230°C.

The carbon black (CB) was Ketjenblack EC 600JD from AKZO NOBEL (Amersfoort, the Netherlands). According to the supplier, the electrical conductivity was 10–100 S/cm, the aggregate size was 30–100 nm, and the apparent bulk density was 1–1.2 g/cm^3.

Compounding

PP and CB were mixed in a Brabender kneader at 200°C and 60 rpm. First, PP was run for 2 min to ensure thorough melting, CB was then added in three equal parts, and the blend was compounded at 100 rpm for 10 min. The CB was dried under vacuum at 120°C for 3 h before compounding. The density of the resulting compound was 0.950 g/cm^3 in the solid state and 0.769 g/cm^3 in the molten state (at 230°C).

Melt spinning

Yarns were produced on a melt spinning line manufactured by Extrusion Systems Limited (ESL), Leeds, England. Figure 1 shows the principle of this spinning line, which is set up for bicomponent spinning: polymer is melted in two separate 18-mm single-screw extruders and metered to the spinneret via two gear pumps, one for the sheath material and one for the core material. A feedback control system ensures constant inlet pressure to the gears.

For PVDF yarns, the same polymer was fed into both extruders, and the temperature settings were as follows:

Extruder zones 1, 2, and 3: 200, 240, and 260°C, respectively.

The spinneret used had 24 holes with a diameter, D_0, of 0.6 mm and a length, L, of 1.2 mm ($L/D_0 = 2$). The temperature of the drawing rollers Nos. 1 and 3 was room temperature. The velocity of drawing roller No. 1 (V_1) was set to $0.95 \cdot V_2$, where V_2 is the velocity of drawing roller No. 2. The exit speed from the die (V_0), the velocity of drawing roller No. 3 (V_3), the temperature of drawing roller No. 2 (T_2) as well as V_1 and V_2 were varied to produce a number of different yarns (refer Table I), as follows:

$$\text{MDR} = V_1/V_0 \tag{1}$$

$$\lambda = V_3/V_2 \tag{2}$$

$$\dot{\varepsilon}_m = (V_1 - V_0)/x \tag{3}$$

where $\dot{\varepsilon}_m$ is the nominal melt deformation rate in min^{-1} and $x = 1.5$ m (i.e., the distance between roller No. 1 and the spinneret exit).

The nominal solid state deformation rate ($\dot{\varepsilon}_{ss}$) is given in min^{-1} and is calculated as

$$\dot{\varepsilon}_{ss} = (V_3 - V_2)/y \tag{4}$$

where $y = 0.325$ m, that is, the distance between the drawing rollers Nos. 2 and 3. Finally, the yarn dimension is given in dtex (grams per 10,000 m) and calculated as

$$\text{dtex} = (\text{mass flow rate} \cdot 10,000)/V_3 \tag{5}$$

For bicomponent yarns, PVDF was used as sheath and CB/PP, with 8.5% CB by weight, constituted the core material. Yarns were spun with two different sheath/core volume ratios: 12/3 and 8/4. The spinneret used had 48 holes with a diameter of 0.6 mm. The settings for the core extruder were

Extruder zones 1, 2, and 3: 210, 240, and 250°C, respectively.

For the sheath extruder the settings were as follows:

Extruder zones 1, 2, and 3: 210, 250, and 260°C, respectively.

The temperature of the metering pumps and of the spinneret was set to 260°C. Because these yarns had low drawability, they were collected on drawing roller No. 1 (see Fig. 1) and then removed from the machine. Cold drawing was done separately.

Cold drawing (off-line)

Cold drawing is drawing in the solid state and is done at a temperature above T_g but below T_m. Some of the PVDF yarns and all the bicomponent yarns were cold-drawn in a separate step using two godets

TABLE I
Spinning Parameters for PVDF Yarns

Yarn	MDR	λ	*T2*	V_0	V_2	V_3	$\dot{\varepsilon}_m$	$\dot{\varepsilon}_{ss}$	dtex/filament
PVDF-20-1	20	1	80	7.1	142	142	90	0	200
PVDF-20-2	〃	2	〃	〃	〃	284	〃	437	100
PVDF-20-3-80	〃	3	〃	〃	〃	425	〃	869	67
PVDF-20-4	〃	4	〃	〃	〃	566	〃	1310	50
PVDF-20-3-60	〃	3	60	〃	〃	425	〃	869	67
PVDF-20-3-70	〃	〃	70	〃	〃	〃	〃	〃	〃
PVDF-20-3-90	〃	〃	90	〃	〃	〃	〃	〃	〃
PVDF-20-3-100	〃	〃	100	〃	〃	〃	〃	〃	〃
PVDF-40-1	40	1	80	3.5	142	142	92	0	100
PVDF-40-2	〃	2	〃	〃	〃	284	〃	437	50
PVDF-40-3	〃	3	〃	〃	〃	425	〃	869	33
PVDF-40-4	〃	4	〃	〃	〃	566	〃	1310	25
PVDF-85-1	85	1	80	3.5	300	300	198	0	47
PVDF-85-2	〃	2	〃	〃	〃	600	〃	923	24
PVDF-85-2.5	〃	2.5	〃	〃	〃	740	〃	1356	19
PVDF-141-1	141	1	80	3.5	500	500	331	0	28
PVDF-141-1.6	〃	1.6	〃	〃	〃	800	〃	923	18

The 〃 symbol means that the value is the same as in the line above.

from Fourné Polymertechnik GmbH (Alfter, Germany). For PVDF yarns, the surface temperature of the first godet was set to 80°C ± 2°C, and for bicomponent yarns, it was set to 100°C ± 2°C. The surface temperature of the second godet was 23°C ± 2°C. The speeds of the godets (V_1 and V_2) could be varied individually between 3 and 28 m/min. The godets were placed 395 mm apart.

Differential scanning calorimetry

DSC analyses were carried out using a TA Instruments (New Castle, Delaware) DSC Q2000. Specimens were prepared from 2 to 4 mg of yarn and placed in an aluminum sample holder which was crimped closed. Scans were carried out at 60–220°C, at a heating rate of 10°C/min. Results shown are from the first heating. They were analyzed using TA Instruments software Universal Analysis 2000. The degree of crystallinity as a percentage (X_c) was calculated as

$$X_c = (\Delta H_m / \Delta H_m^0) \cdot 100\% \quad (6)$$

where ΔH_m is the experimental heat of fusion, and ΔH_m^0 is the heat of fusion of the 100% crystalline polymer. The value of ΔH_m^0 for PVDF was taken to be 104.7 J/g,[21] and ΔH_m was calculated from the area of the endothermic melting peak. DSC measurements were made on at least three specimens from each yarn.

X-ray diffraction

X-ray diffractograms were obtained using a Bruker AXS (Madison, Wisconsin) D8 Advance Theta X-ray diffractometer with monochromator. The radiation source was Cr Kα with a wavelength of 2.28970 Å. An increment step of 0.1° at a rate of one step per 10 s was used. During the measurement, the sample was rotating at 30 rpm. All measurements were made at room temperature. Samples consisted of parallel fibers mounted on a flat sample holder by means of double-sided adhesive tape. Fibers were mounted, so that they covered the whole surface of the sample holder. XRD measurements were made on several samples of fibers. Although there was some variation in the sizes of the peaks, the trends remained unchanged and were clear. There was good repeatability in the positions of the peaks; diffractograms displayed in the article are representative of these measurements.

Electrical conductivity measurements

Electrical properties of the bicomponent yarns were measured by a two-point set up, as illustrated in

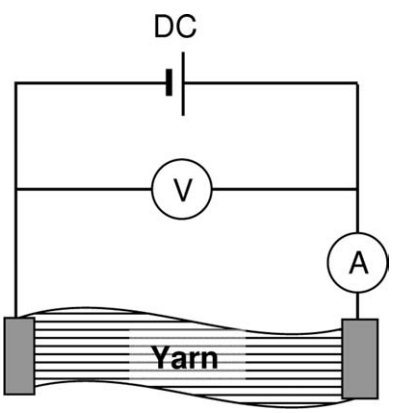

Figure 2 Setup for conductivity measurements.

TABLE II
Interplanar distances for maximum intensity peaks found in PVDF, according to the literature

α-Phase[1,4–8]			β-Phase[1,4–7,9,10]		
hkl	*d* (Å)	2Θ	hkl	*d* (Å)	2Θ
110	4.39–4.45	29.8°–30.2°	110/200	4.23–4.33	30.7°–31.4°
200	4.79–4.82	27.5°–27.7°			
010	4.92–5.10	26.0°–26.9°			

The corresponding 2Θ angles were calculated for λ = 0.22897 nm.

Figure 2. Specimens of ~ 0.2 g were prepared by collecting a bundle of yarns, cutting them with a razor blade, and applying electrodes on each end by means of silver paint. The silver paint was allowed to wet the ends and the outer parts of the yarn thoroughly to ensure good contact with the conductive core material of each filament. A power supply, D400-007D from Oltronix (Em Leek, the Netherlands), was used to apply a voltage (denoted DC in Fig. 2), which was measured by a voltmeter (V) Fluke 111 True RMS multimeter from Fluke (Solna, Sweden). The current (A) was measured by a 602 Solid state Electrometer from Keithley Instruments (Ohio, USA). The voltage was varied in steps from 10 to 160 V, and the resulting current was recorded. From the measurements, the volume conductivity (σ_v) was considered to be independent of voltage, and the results given here are average values. σ_v was calculated as

$$\sigma_v = I\rho l^2/(Um) \quad (7)$$

where U is the measured voltage, m is the mass of the core material, I is the measured current, ρ is the density of the core material, and l is the length of the sample between the silver paint contacts. Thus, the calculated conductivity refers only to the core part of the yarns.

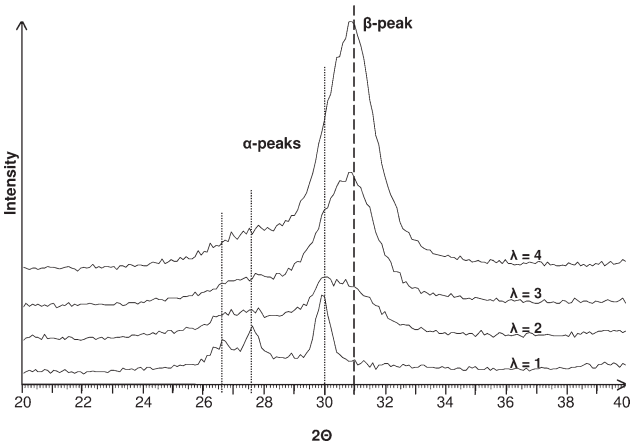

Figure 3 X-ray diffractograms for yarns spun with MDR = 20 before and after cold drawing.

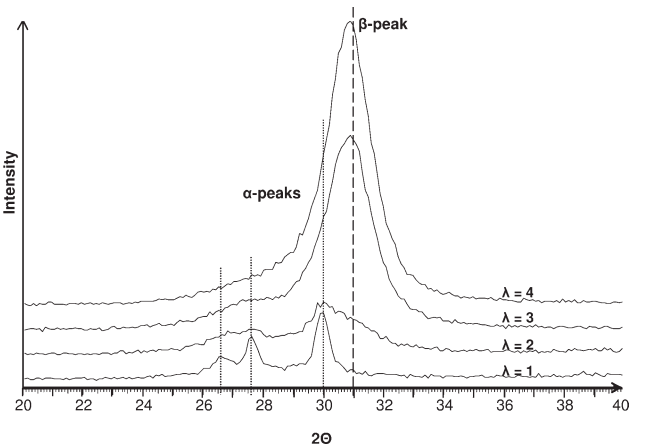

Figure 4 X-ray diffractograms for yarns spun with MDR = 40 before and after cold drawing.

RESULTS AND DISCUSSION

Melt spinning of PVDF yarns

Figure 3 shows the XRD diffractograms for yarns spun with MDR = 20. Peaks found can be attributed to α- and β-phase crystallites as referred to in Table II. It can be seen that, as λ increases, the relative amount of β-phase crystallinity increases. The same trend is found in Figures 4–6. All the yarns were cold drawn up to the maximum available λ. In summary, the results presented in Figures 3–6 confirm the important points found in our previous study[12]: (i) cold drawing is necessary to introduce the β-phase, (ii) the relative amount of β-phase crystallinity increases with increasing λ, (iii) the maximum available λ, and thus the maximum relative amount of β-phase, decreases with increasing MDR.

Figures 7 and 8 show representative DSC-thermograms for yarns before and after cold drawing. As can be seen, there was no significant change in the appearance of the peaks after cold drawing. In Figure 9, the dependence of X_c, as calculated from the

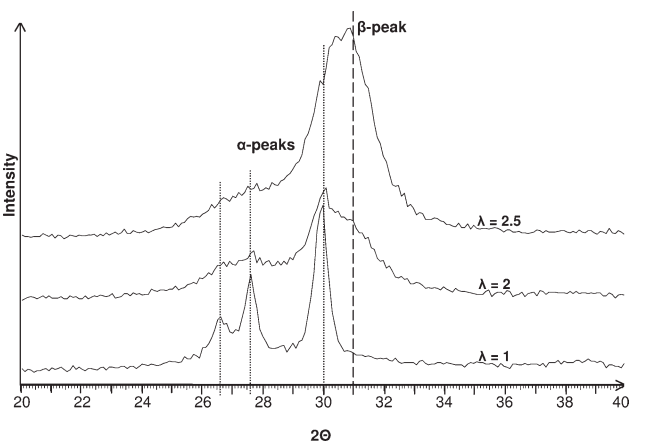

Figure 5 X-ray diffractograms for yarns spun with MDR = 85 before and after cold drawing.

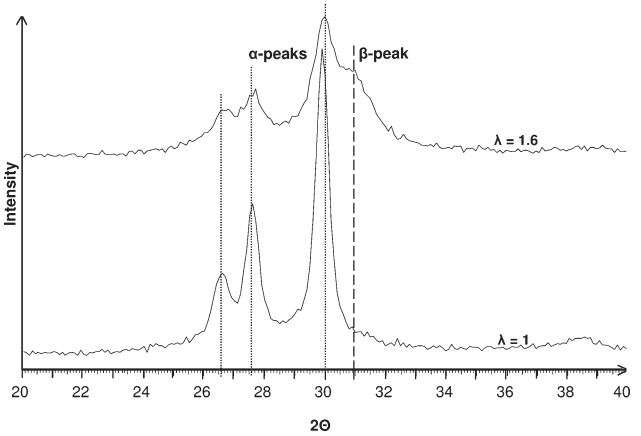

Figure 6 X-ray diffractograms for yarns spun with MDR = 141 before and after cold drawing.

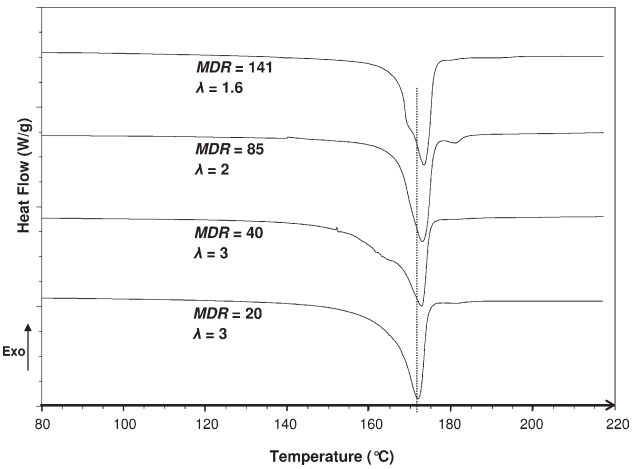

Figure 8 Representative DSC thermograms for yarns after cold drawing.

DSC-measurements, on λ and MDR is shown. The graph shows a weak trend toward increasing X_c with increasing λ. In our previous paper,[12] no such increase was found. The present results may be explained by the fact that, as can be seen in Figure 10, X_c increases slightly with increasing $\dot{\varepsilon}_{ss}$ (which is 10–100 times higher in large-scale spinning than in the laboratory-scale spinning used earlier). It should be noted that the maximum standard deviation for X_c is ±4.9%.

Figure 9 also shows that X_c in the yarns is between 53 and 63%, which is close to the X_c of PVDF homopolymer as given by the supplier (56–61%). This seems low compared to our previous experiments,[12] where it was found that at low values for MDR (42 and 84) X_c were 60%, followed by a strong increase to 80–90% at high MDRs of 251 and 419. This may be due to the larger scale spinning, where X_c is slightly lower due to the relatively high-drawing speeds and smaller filament diameter, which will lead to faster cooling of the filaments. Furthermore, in the large-scale spinning trials, the maximum MDR was lower, around 141.

Another limitation of the large-scale production stems from the spinning machine equipment. In the present experiments, it was not possible to use the same grade of (relatively high-molecular weight, MW) PVDF, because this resulted in visible melt instabilities, namely, sharkskin and spinline break. This was solved practically by choosing a lower MW/lower viscosity grade PVDF and using a higher processing temperature. The main explanation of these limitations may be found in the extrusion rates and die geometries. In the ESL machine used for large-scale spinning, the available extrusion rates were relatively high; 3.5 and 7.1 m/min instead of 0.45 m/min in the laboratory experiments. The ESL die consists of a spin-pack with several layers, where, for each layer, the melt is pumped through a converging channel into a thinner capillary; the final capillary has a 90° conical entrance. In the small-

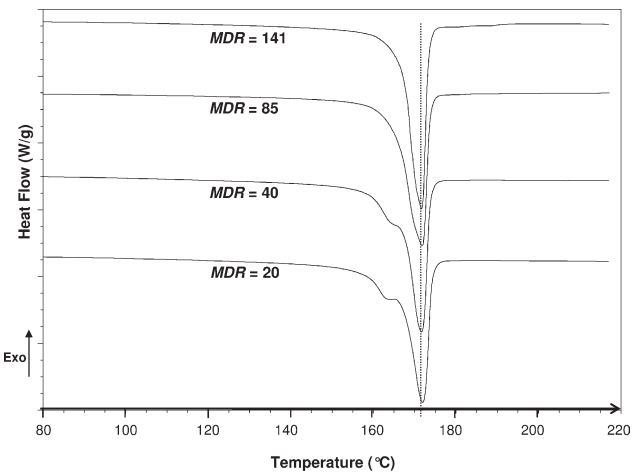

Figure 7 Representative DSC thermograms for yarns drawn only in the melt.

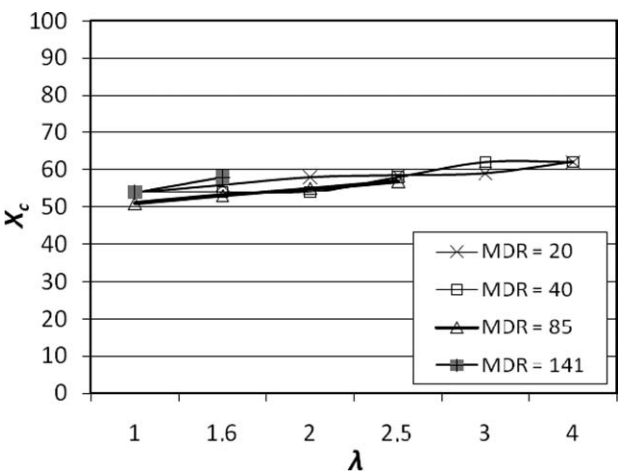

Figure 9 Degree of crystallinity as a function of λ for different MDRs.

TABLE III
Yarns and Parameters Used for Off-Line Cold Drawing

Yarn	*MDR*	λ	Temperature godet 1 (°C)	Speed godet 1 (m/min)	Speed godet 2 (m/min)	$\dot{\varepsilon}_{ss}$
PVDF-20-1	20	1	80	–	–	0
PVDF-20-3-ε15	″	3	″	3	9	15
PVDF-20-3-ε30	″	″	″	6	18	30
PVDF-40-1	40	1	80	–	–	0
PVDF-40-3-ε15	″	3	″	3	9	15
PVDF-40-3-ε30	″	″	″	6	18	30

The ″ symbol means that the value is the same as in the line above.

scale spinning device, the die consisted of a single capillary with a flat (180°) entrance. Compared to our small-scale spinning device, the final capillary of the ESL die had a smaller diameter D_0 (0.6 mm instead of 1 mm) and a smaller L/D_0 ratio (2 instead of 40). These factors affect the degree of preorientation in the melt. The spinnability, or drawability, of a melt may be characterized by the maximum draw-down speed and force. Spinnability depends on the elongational viscosity level as well as on the state of orientation of the melt when it leaves the die.[22]

Melt fracture is affected by the same viscoelastic memory mechanisms as die swell phenomena and depends in a similar way on material characteristics and extrusion conditions. High swelling usually occurs just before the outflow becomes irregular. Thus, although in spinning the die swell is largely suppressed by drawing of the melt, the mechanisms leading to large die swell ratios can be considered to be an indication of coming melt fracture.[23] The die design has a strong influence on the die swell and drawability. In the converging part of a die, elongational strains are imposed. If the melt subsequently flows through a parallel channel, relaxation will occur, so that the orientations decay and contribute less to the swelling. The degree of relaxation increases with increasing channel length. It is also highly dependent on the MW, as a high-MW polymer will have a longer relaxation time. Thus, depending on these conditions, the melt exiting from the die may have a pronounced uniaxial preorientation, which will result in a drastic reduction in the maximum draw-down speed and ratio.[22] The highest degree of melt orientation in the capillary occurs near the walls, and the degree of die swell increases with increasing wall shear rate in the capillary ($\dot{\gamma}_w$),[22,24] which is calculated as

$$\dot{\gamma}_w = 4Q/(\pi r^3) \tag{8}$$

where Q is the volumetric flow rate and r is the radius of the capillary. $\dot{\gamma}_w$ in our small-scale spinning experiments was ~ 10 times lower than in the large-scale spinning.

Sharkskin is another form of distortion in an extruded melt, possibly caused by cohesive failure near the surface. It is initiated at the die exit by the sudden and large axial acceleration of the melt layer next to the capillary wall. For a given polymer, sharkskin will occur above a certain maximum flow rate, the level of which has been found to be lower in a polymer with lower MFI.[24]

In the cold drawing of PVDF-films to produce the β-phase, it has been reported that a high $\dot{\varepsilon}_{ss}$

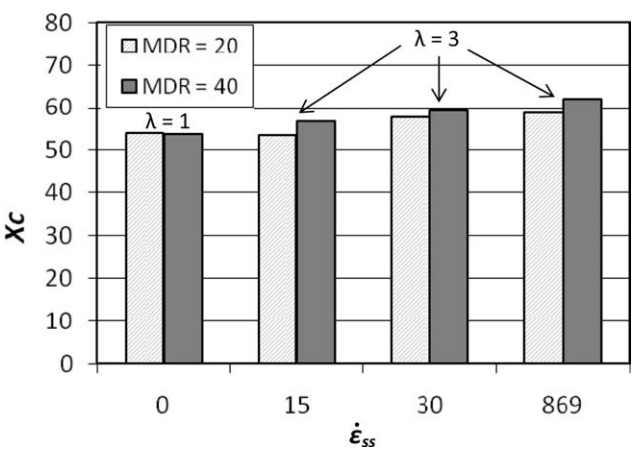

Figure 10 X_c as a function of $\dot{\gamma}_{ss}$ for PVDF yarns spun with MDR = 20 and 40.

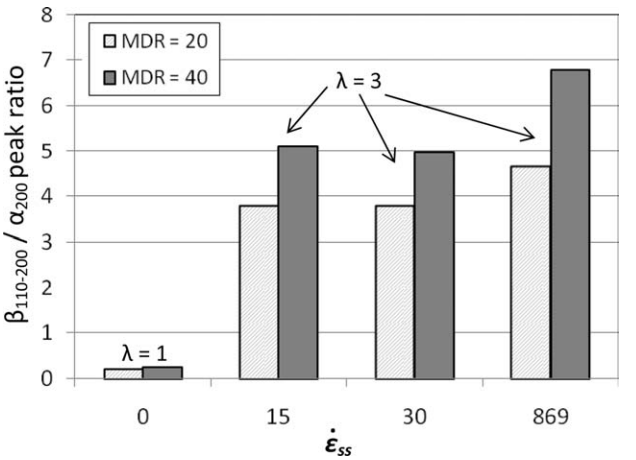

Figure 11 $\beta_{110–200}/\alpha_{200}$ peak ratio related to $\dot{\varepsilon}_{ss}$ for yarns spun with MDR = 20 and 40.

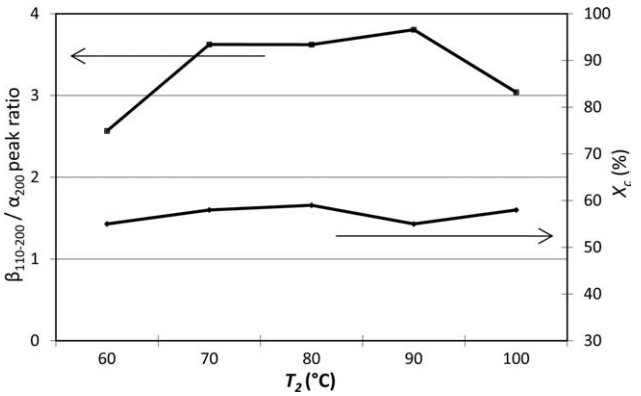

Figure 12 $\beta_{110–200}/\alpha_{200}$ peak ratio and X_c related to T_2, for yarns spun with MDR = 20 and λ = 3.

promotes α-to-β-phase conversion.[11,25,26] This is due to the shorter time for stress relaxation, compared to drawing at low $\dot{\varepsilon}_{ss}$. To study this effect in yarns, cold drawing was done off-line using a relatively low $\dot{\varepsilon}_{ss}$, as listed in Table III. This was done on yarns spun at MDR = 20 and 40, with λ = 1. In Figure 10, X_c is shown as a function of $\dot{\varepsilon}_{ss}$ for the yarns and yarns spun with the same MDRs and in-line drawing (where $\dot{\varepsilon}_{ss}$ is much higher). As has already been mentioned, there is a slight increase in X_c with increasing $\dot{\varepsilon}_{ss}$. In Figure 11, the degree of α-to-β-phase conversion is shown as the ratio between the maximum intensities, respectively, of the two peaks $\beta_{110–200}$ (at 31°) and α_{200} (at 27.6°). This is a way to semiquantify the XRD-curve, which should not be confused with the β-to-α-phase ratio, which can only be qualitatively estimated from the diffractograms and has thus not been calculated. The results show that an increase in $\dot{\varepsilon}_{ss}$ increases the β-to-α-peak ratio and that the effect is more pronounced in the yarns spun with the higher MDR. However, it is clear that λ has a much higher impact than $\dot{\varepsilon}_{ss}$ on α-to-β-phase conversion.

The possible effect of the temperature used in cold drawing has also been investigated. Yarns with MDR = 20 and λ = 3 were drawn in-line at T_2 set to 60, 70, 80, 90, and 100°C. The results from XRD are shown in Figure 12 as the $\beta_{110–200}/\alpha_{200}$ ratio, and the optimal drawing temperature for maximum α-to-β-phase conversion was found to be between 70 and 90°C. This is similar to other reports on the drawing of PVDF films[25,26] and fibers.[27] In drawing, the applied stress can cause imperfect α-crystallites to be reorganized and transformed into the β-phase. At lower stretching temperatures, the transformation mechanism is relatively weak, but above a certain temperature, the stress introduced by drawing will be relatively low due to the increase in chain mobility.[27] Thus, it is possible to identify an optimum processing window for the transformation to take place. At temperatures above 140°C, there will be no α-to-β-transformation, because the high-chain mobility will result in recrystallization to form the kinetically favored α-phase.[28] As is also shown in Figure 12, X_c was not significantly affected by the drawing temperature.

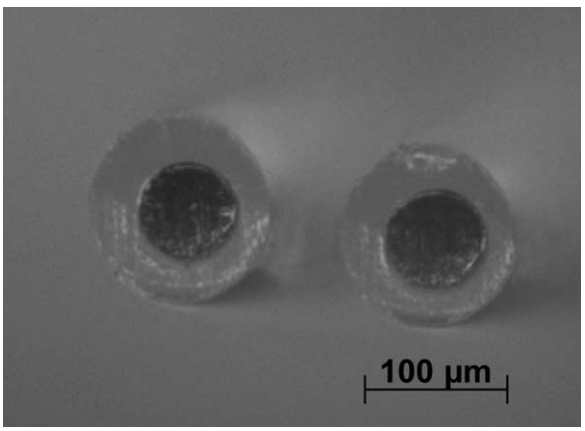

Figure 13 Photomicrograph of two single bicomponent filaments spun with a 8/4-volume-ratio between sheath and core. MDR = 25, λ = 1.

Melt spinning of bicomponent PVDF yarns with a conductive core

Conductive fibers can be melt spun by including conductive particles, for example, CB, in the polymer melt. To achieve conductivity in such a compound, a sufficient amount of particles must be added to form a percolating network within the

TABLE IV
Parameters Used in Bicomponent Yarn Spinning and Cold Drawing

Yarn	MDR	λ	Flow rate core (cm^3/min)	Flow rate sheath (cm^3/min)	V_0	V_1	Temperature godet 1 (°C)	Speed godet 1 (m/min)	Speed godet 2 (m/min)	$\dot{\varepsilon}_{ss}$
Bicomp-12/3-20-1	20	1	7.2	28.8	2.65	50	100	–	–	0
Bicomp-12/3-20-2	〃	2	〃	〃	〃	〃	〃	3	6	15
Bicomp-12/3-20-3	〃	3	〃	〃	〃	〃	〃	〃	9	30
Bicomp-8/4-25-1	25	1	9.6	19.2	2.12	〃	〃	–	–	0
Bicomp-8/4-25-2	〃	2	〃	〃	〃	〃	〃	3	6	15
Bicomp-8/4-25-3	〃	3	〃	〃	〃	〃	〃	〃	9	30

The 〃 symbol means that the value is the same as in the line above.

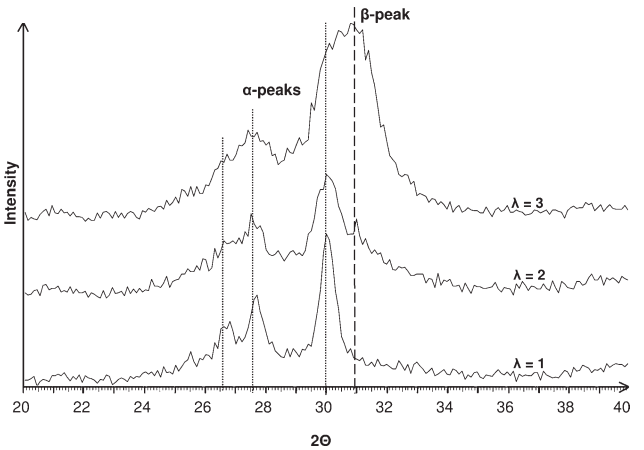

Figure 14 X-ray diffractograms for bicomponent yarns spun with a 12/3-volume-ratio between sheath and core. MDR = 20.

polymer matrix. However, this will also lead to a change in the rheological properties of the melt, and, as a consequence, the spinnability is usually lower. In polymer melts containing small particles, spinline instabilities can occur as fluctuations in the fiber diameter already at low MDRs, and, above a critical *MDR*, these fluctuations occur more frequently and become larger in amplitude. The elongation to break is significantly reduced.[29]

Bicomponent spinning of sheath/core type fibers may be used for spinning fibers where one component (the core) cannot normally be spun, due to, for example, a very low viscosity or a highly elastic behavior.[30,31] In this section, we present early results from the spinning of bicomponent yarns with a core/sheath structure, as a means of adding an inner electrode to the PVDF yarns. The choice of core material in this work, PP with 8.5% CB, was based on previous experience.[32] The percolation threshold for

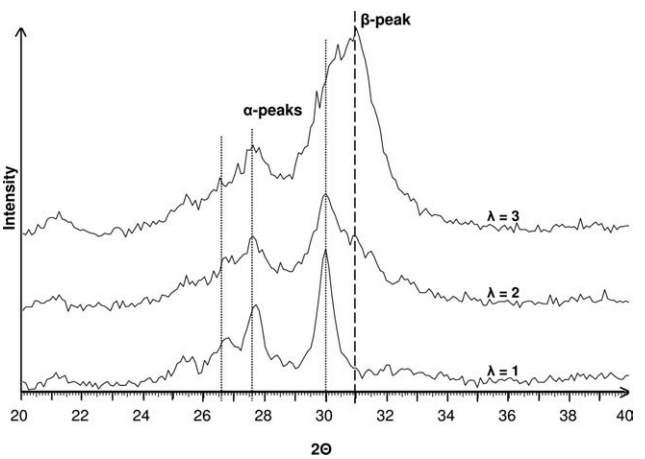

Figure 15 X-ray diffractograms for bicomponent yarns spun with an 8/4-volume-ratio between sheath and core. MDR = 25.

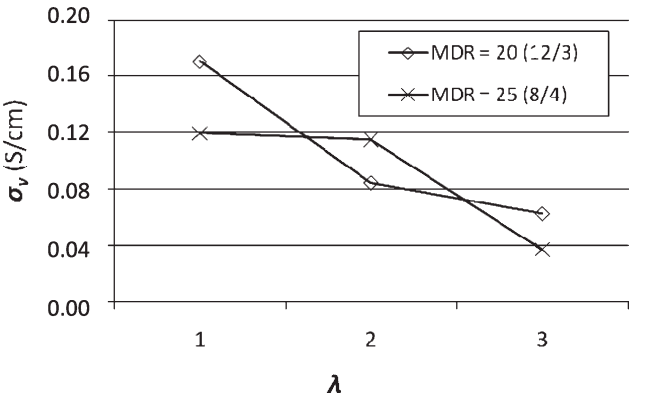

Figure 16 σ_v of bicomponent yarns as a function of λ, with different sheath/core volume ratios.

this compound is at ~ 2% CB by weight, and at 8.5% by weight a conductivity of 0.2 S/cm can be expected. Figure 13 shows the cross sections of two single filaments from the bicomponent yarns with an 8/4 sheath/core volume ratio.

It was found that fibers could be spun without spinline breakage, only at low MDRs (20–25), and it was not possible to carry out cold drawing in-line. Instead, this was done separately. The conditions used for melt spinning and cold drawing are listed in Table IV. XRD diffractograms for the bicomponent fibers before and after drawing are shown in Figures 14 and 15. Drawing at λ = 3 introduced β-phase crystallites in the yarns, but the β-to-α-phase ratio seemed to be less than in the PVDF yarns with the same MDR and λ (see Fig. 3). This can be explained, as previously discussed, by the lower draw rate used for the bicomponent fibers, combined with the higher drawing temperature; the temperature of godet 1 had to be set to 100°C to reduce yarn breakage.

The results of the conductivity measurements are shown in Figure 16. The σ_v of undrawn yarns was in the range of 0.12–0.18 S/cm and decreased with increasing λ. This is probably due to a destruction of the conductive network during drawing. There was no significant difference in the σ_v between yarns with different sheath/core volume ratios. Earlier results[31] have shown that the heat treatment of conductive bicomponent fibers with the same core material at 180°C is an efficient way to substantially improve σ_v. Because the Curie transition, where polarity will be lost, is expected to commence near the melting point of PVDF[33] (around 173°C), it seems probable that such a heat treatment would destroy the necessary β-phase in our yarns.

To increase the drawability and to enable heat treatment, further experiments regarding the optimal composition of the core compound as well as the sheath/core volume ratio are required. This will be investigated in a separate study.

CONCLUSIONS

Experimental results from the melt spinning of PVDF under conditions typical for industrial-scale fiber production are presented. It is shown that it is possible to melt-spin bicomponent fibers with β-phase PVDF in the sheath and a CB/PP compound in the core. The core material was electrically conductive and can thus be used as an inner electrode. It was found that, for maximum α-to-β phase transformation, which takes place during cold drawing, the surface temperature of the drawing wheel should be between 70 and 90°C and that both the draw ratio and the draw rate should be as high as possible. An increase in the MDR will decrease the maximum possible draw ratio in cold drawing. Therefore, the melt draw ratio should be kept low.

References

1. Lando, J. B.; Doll, W. W. J Macromol Sci Phys 1968, B2, 205.
2. Weinhold, S.; Litt, M. H.; Lando, J. B. Macromolecules 1980, 13, 1178.
3. Bachmann, M.; Gordon, W. L.; Weinhold, S.; Lando, J. B. J Appl Phys 1980, 51, 5095.
4. Wang, Y.; Cakmak, M.; White, J. L. J Appl Polym Sci 1985, 30, 2615.
5. Matsushige, K.; Nagata, K.; Imada, S.; Takemura, T. Polymer 1980, 21, 1391.
6. Das Gupta, D. K.; Doughty, K. Appl Phys Lett 1977, 31, 585.
7. Zhang, H.; Ren, P.; Zhang, G.-F.; Xiao, C.-F. J Wuhan Univ Technol 2006, 21, 53.
8. Li, X.; Lu, X. J Appl Polym Sci 2007, 103, 935.
9. Hasegawa, R.; Takahashi, Y.; Chatani, Y.; Tadokoro, H. Polym J 1972, 3, 600.
10. Teulings, R. P.; Dumbleton, J. H.; Miller, R. L. Polym Lett 1968, 6, 441.
11. Mohammadi, B.; Yousefi, A. A.; Bellah, S. M. Polym Test 2007, 26, 42.
12. Lund, A.; Hagström, B. J Appl Polym Sci 2010, 116, 2685.
13. Jadidian, B.; Allahverdi, M.; Mohammadi, F.; Safari, A. J Electroceram 2002, 8, 209.
14. Sato, H.; Takagi, K.; Yu, L.; Nagamine, M. Mater Res Soc Symp Proc 2006, 888, V01.
15. Mohammadi, F.; Khan, A.; Cass, R. B. Mater Res Soc Symp Proc 2003, 736, 263.
16. Pini, N.; Busato, S.; Elsener, H.-R.; Ermanni, P. Polym Adv Technol 2007, 18, 249.
17. Wang, T. T.; Herbert, J. M.; Glass, A. M., Eds. The Applications of Ferroelectric Polymers; Kluwer: Boston, 1988.
18. Measurement Specialties, L. W., Hampton, VA23666, USA.
19. Mazurek, B.; Rózecki, S.; Kowalczyk, D. The 6th International Conference on Properties and Applications of Dielectric Materials, Xi'an Jiaotong University, Xi'an, China, 2000; p 1041.
20. Mazurek, B.; Rózecki, S.; Kowalczyk, D.; Janiczek, T. J Electrostat 2001, 51–52, 180.
21. Wang, Y. D.; Cakmak, M. J Appl Polym Sci 1998, 68, 909.
22. Laun, H. M.; Schuch, H. J Rheol 1989, 33, 119.
23. Ziabicki, A. Fundamentals of Fibre Formation; Wiley: Bath, 1976.
24. Tadmor, Z.; Gogos, C. G. Principles of Polymer Processing; Wiley: New York, 2006.
25. Sobhani, H.; Razavi-Nouri, M.; Yousefi, A. A. J Appl Polym Sci 2007, 104, 89.
26. Sajkiewicz, P.; Wasiak, A.; Goclowski, Z. Eur Polym J 1999, 35, 423.
27. Du, C.-H.; Zhu, B.-K.; Xu, Y.-Y. J Appl Polym Sci 2007, 104, 2254.
28. Wu, J.; Schultz, J. M.; Yeh, F.; Hsiao, B. S.; Chu, B. Macromolecules 2000, 33, 1765.
29. White, J. L.; Tanaka, H. J Appl Polym Sci 1981, 26, 579.
30. Hagström, B. The Polymer Processing Society Europe/Africa Regional Meeting—PPS-2009, Larnaca, Cyprus, October 18–21, 2009.
31. Stråat, M.; Hagström, B. Unpublished results: 2010.
32. Hagström, B. Ambience08, Borås, Sweden, 2008; p 20.
33. Lovinger, A. J.; Furukawa, T.; Davis, G. T.; Broadhurst, M. G. Ferroelectrics 1983, 50, 227.